

## Aberystwyth University

### *Diffraction of antiplane shear waves and stress concentration in a cracked couple stress elastic material with micro inertia*

Nobili, Andrea; Radi, Enrico; Vellender, Adam

*Published in:*

Journal of the Mechanics and Physics of Solids

*DOI:*

[10.1016/j.jmps.2018.11.013](https://doi.org/10.1016/j.jmps.2018.11.013)

*Publication date:*

2019

*Citation for published version (APA):*

Nobili, A., Radi, E., & Vellender, A. (2019). Diffraction of antiplane shear waves and stress concentration in a cracked couple stress elastic material with micro inertia. *Journal of the Mechanics and Physics of Solids*, 124, 663-680. <https://doi.org/10.1016/j.jmps.2018.11.013>

#### **General rights**

Copyright and moral rights for the publications made accessible in the Aberystwyth Research Portal (the Institutional Repository) are retained by the authors and/or other copyright owners and it is a condition of accessing publications that users recognise and abide by the legal requirements associated with these rights.

- Users may download and print one copy of any publication from the Aberystwyth Research Portal for the purpose of private study or research.
- You may not further distribute the material or use it for any profit-making activity or commercial gain
- You may freely distribute the URL identifying the publication in the Aberystwyth Research Portal

#### **Take down policy**

If you believe that this document breaches copyright please contact us providing details, and we will remove access to the work immediately and investigate your claim.

tel: +44 1970 62 2400

email: [is@aber.ac.uk](mailto:is@aber.ac.uk)

# Diffraction of antiplane shear waves and stress concentration in a cracked couple stress elastic material with micro inertia

Andrea Nobili<sup>a</sup>, Enrico Radi<sup>b</sup>, Adam Vellender<sup>c</sup>

<sup>a</sup>*Dipartimento di Ingegneria Enzo Ferrari, via Vivarelli 10, 41125 Modena, Italy*

<sup>b</sup>*Dipartimento di Scienze e Metodi dell'Ingegneria, via Amendola 2, 42122 Reggio Emilia, Italy*

<sup>c</sup>*Institute of Mathematical and Physical Sciences, Aberystwyth University, Ceredigion SY23 3BZ, Wales, UK.*

---

## Abstract

We investigate diffraction of reduced traction shear waves applied at the faces of a stationary crack in an elastic solid with microstructure, under antiplane deformation. The material behavior is described by the indeterminate theory of couple stress elasticity and the crack is rectilinear and semi-infinite. The full-field solution of the crack problem is obtained through integral transforms and the Wiener-Hopf technique. A remarkable wave pattern appears which consists of entrained waves extending away from the crack, reflected Rayleigh waves moving along the crack, localized waves irradiating from the crack-tip with, possibly, super-Rayleigh speed and body waves scattered around the crack-tip. Interestingly, the localized wave solution may be greatly advantageous for defect detection through acoustic emission. Dynamic stress intensity factors are presented, which generalize to Elastodynamics the corresponding results already obtained in the static framework. The correction brings out the important role of wave diffraction on stress concentration.

**Keywords:** Couple stress, Wave diffraction, Rayleigh waves, Dynamic stress intensity factor

---

\*Corresponding author

## 1. Introduction

The study of wave diffraction has attracted major interest since its discovery, in the XVII century, by Francesco Maria Grimaldi in the context of light wave propagation (see Mow and Pao (1971) for an excellent historical account). Indeed the term diffraction was then introduced to indicate a deviation from the rectilinear path which could not be accounted for by either reflection or refraction. Starting from the pioneering work by Clebsch (1863) and Rayleigh (1896), diffraction of elastic waves by inclusions, barriers and obstacles has been investigated in a vast body of literature. Nonetheless, only in fairly recent times the importance of dynamic effects in determining the stress concentration in the presence of geometric discontinuities could be appreciated. Indeed, “dynamic stress concentration is a result of diffraction of elastic wave” (Mow and Pao, 1971).

Elastic wave diffraction and stress concentration are almost always investigated within the classical theory of Elastodynamics, which fails to account for the discontinuous nature of many engineering materials, the so-called microstructure. As an example, this theory cannot predict dispersion of Rayleigh waves at high frequency, when the wavelength becomes comparable to the material characteristic length (Georgiadis and Velgaki, 2003). Besides, the discrepancy between the classical theory and the experimental evidence is more pronounced for those complex materials, such as composites, cellular materials, foams, masonry, bone tissues, glassy and semicrystalline polymers, for which modelling is most needed. In this respect, wave diffraction and microstructural effects are deeply related to each other and together contribute to the determination of the stress concentration near geometric discontinuities.

The use of enhanced constitutive models based on strain gradient or nonlocal theories of elasticity allows to circumvent some of the pathological results provided by the classical theory of elasticity (Georgiadis and Vardoulakis, 1998). However, the number of material parameters is comparatively large (Mindlin, 1964; Mindlin and Eshel, 1968; Lam, Yang, Chong, Wang, and Tong, 2003), so

31 that a substantial effort is required on the experimental side for their determi-  
 32 nation Maranganti and Sharma (2007). Furthermore, analytical solutions are  
 33 most often inaccessible (Gao and Ma, 2010).

34 An intermediate step between the classical elastic theory and the most ad-  
 35 vanced strain gradient theories is provided by the Cosserat micropolar model,  
 36 which involves only rotational gradients (Graff and Pao, 1967). A special class of  
 37 micropolar theories is represented by the indeterminate couple stress (CS) the-  
 38 ory, developed by Koiter (1964) for the quasi-static regime and later extended  
 39 by Eringen (1999) to Elastodynamics. Alongside the traditional Lamé moduli,  
 40 this elastic constitutive model features two extra material characteristic lengths,  
 41 associated to bending and torsion, as well as the micropolar rotatory inertia.

42 Comparably few contributions can be found in the literature discussing wave  
 43 propagation in solids with microstructure. The original contribution by Graff  
 44 and Pao (1967) considers wave reflection by a rigid obstacle in a CS half-space  
 45 under plane strain. More recently, a similar treatment is given in Gourgiotis,  
 46 Georgiadis, and Neocleous (2013) for a grade two strain-gradient material fea-  
 47 turing three material constants. Rayleigh waves propagating in CS materials  
 48 are investigated in Ottosen, Ristinmaa, and Ljung (2000), in the absence of  
 49 rotational inertia, and then in Georgiadis and Velgaki (2003) accounting for ro-  
 50 tational inertia, again under plane strain. Scattering of antiplane shear waves  
 51 caused by a cylindrical inclusion within the CS theory is considered by Shodja,  
 52 Goodarzi, Delfani, and Haftbaradaran (2015).

53 Enhanced models of continua may result in new types of surface waves, for  
 54 example the appearance of new surface antiplane waves in a half-space with  
 55 surface stresses (Eremeyev, Rosi, and Naili, 2016). It is also worth noting that  
 56 sometimes different constitutive models may lead to the same qualitative wave  
 57 pattern, as it is shown by Eremeyev, Rosi, and Naili (2018) for antiplane wave  
 58 propagation within the Gurtin-Murdoch surface elasticity or considering the  
 59 Toupin-Mindlin strain-gradient elasticity models.

60 When stress concentration is investigated in microstructured media, it ap-  
 61 pears that all contributions available in the literature deal with static or steady-

state propagating problems. Zhang, Huang, Chen, and Hwang (1998) give the full-field solution and stress intensity factors for the static Mode III crack problem (antiplane deformation) in a reduced CS material with three material parameters (although only two affect the antiplane behaviour). The general solution for indeterminate CS materials is given in Radi (2008). Later, the problem of steady-state Mode III crack propagation has been investigated by Mishuris, Piccolroaz, and Radi (2012); Morini, Piccolroaz, Mishuris, and Radi (2013); Morini, Piccolroaz, and Mishuris (2014). Georgiadis (2003) appears to be the first and only contribution considering dynamic stress concentration in a straight semi-infinite crack in the presence of microstructure, although the latter is accounted for through the simpler grade two strain gradient theory. Besides, the classical linear elastic fracture mechanics field, with time-harmonic variation, is considered in the far field as the forcing term.

In this paper, a travelling wave loading, applied in the form of shear reduced tractions at the crack faces, is considered as the forcing term. As a result, a complicated wave pattern appears, which differs significantly from the classical solution given in Freund (1998). This loading condition may be used as a building block to address, by means of superposition, any wave propagation problem in a cracked CS half-space. Resonance is triggered when the applied loading is fed *into* the crack-tip at Rayleigh speed. Elastodynamic stress intensity factors are given, which generalize the corresponding results presented in Radi (2008) for the static regime. They incorporate the effect of the applied loading frequency and thereby account for the interplay of the diffracted waves.

## 2. Antiplane couple stress elasticity

Let us consider a Cartesian co-ordinate system  $(O, x_1, x_2, x_3)$ , such that the rectilinear crack occupies the semi-infinite line  $x_1 < 0$ , Fig.1. The indeterminate theory of CS elasticity adopted in the present study provides the following kinematical (compatibility) conditions (Koiter, 1964, Eqs.(4.9)) for the strain tensor

$$\varepsilon = \text{Sym grad } \mathbf{u}, \quad (1)$$

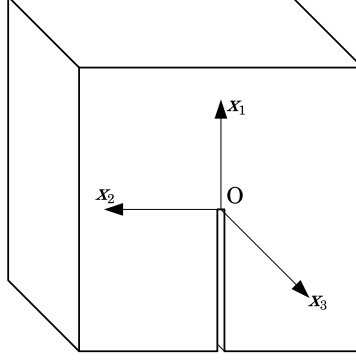


Figure 1: Semi-infinite rectilinear crack  $x_1 < 0$  in a half-space under antiplane deformation along  $x_3$

for the rotation vector

$$\boldsymbol{\varphi} = \frac{1}{2} \text{curl } \mathbf{u}, \quad (2)$$

and for the *torsion-flexure tensor*

$$\boldsymbol{\chi} = \text{grad } \boldsymbol{\varphi}. \quad (3)$$

We observe that, through Eq.(3), micro-rotations are determined by the macro-motion, which feature makes the CS theory a restriction of the micropolar theory. Under antiplane shear deformation, the displacement field  $\mathbf{u} = (u_1, u_2, u_3)$  is completely defined by the out-of-plane component  $u_3 = u_3(x_1, x_2, x_3, t)$ . The nonzero components of the strain, rotation and of the flexure-torsion tensors become

$$\varepsilon_{13} = \frac{1}{2} u_{3,1}, \quad \varepsilon_{23} = \frac{1}{2} u_{3,2}, \quad (4a)$$

$$\varphi_1 = \frac{1}{2} u_{3,2}, \quad \varphi_2 = -\frac{1}{2} u_{3,1}, \quad (4b)$$

$$\chi_{11} = -\chi_{22} = \frac{1}{2} u_{3,12}, \quad \chi_{21} = -\frac{1}{2} u_{3,11}, \quad \chi_{12} = \frac{1}{2} u_{3,22}. \quad (4c)$$

Hereinafter, a subscript comma denotes partial differentiation, e.g.  $u_{3,i} = \partial u_3 / \partial x_i$ .

The Cauchy stress tensor  $\mathbf{t}$  is decomposed into its symmetric and skew-symmetric parts, respectively  $\boldsymbol{\sigma}$  and  $\boldsymbol{\tau}$ ,

$$\mathbf{t} = \boldsymbol{\sigma} + \boldsymbol{\tau}, \quad \boldsymbol{\sigma} = \text{Sym } \mathbf{t}, \quad \boldsymbol{\tau} = \text{Skw } \mathbf{t}.$$

97 In addition, the deviatoric part of the couple stress tensor,  $\boldsymbol{\mu}$ , is introduced as  
 98 being work-conjugated to  $\boldsymbol{\chi}^T$  (Koiter, 1964, Eq.(2.22)). Indeed, the CS theory is  
 99 named indeterminate after the observation that the first invariant of the couple-  
 100 stress tensor, i.e.  $\text{tr } \boldsymbol{\mu} = \mu_{11} + \mu_{22} + \mu_{33}$ , rests indeterminate and therefore it  
 101 may be set equal to zero without loss of generality.

102 At any point of a smooth surface we may specify the *reduced force traction*  
 103 vector  $\mathbf{p}$  and the tangential part of the *couple stress traction* vector  $\mathbf{q}$  (Koiter,  
 104 1964, Eqs.(3.5-6))

$$\mathbf{p} = \mathbf{t}^T \mathbf{n} + \frac{1}{2} \text{grad } \mu_{nn} \times \mathbf{n}, \quad \mathbf{q} = \boldsymbol{\mu}^T \mathbf{n} - \mu_{nn} \mathbf{n}, \quad (5)$$

105 where we have  $\mu_{nn} = \mathbf{n} \cdot \boldsymbol{\mu} \mathbf{n} = \mathbf{q} \cdot \mathbf{n}$ . In particular, at the bottom/top crack  
 106 face  $x_2 = 0^\mp$ , it is  $\mathbf{n} = \pm(0, 1, 0)$  and, according to Eqs.(5), the out-of-plane  
 107 component of the reduced force traction and the in-plane components of the  
 108 couple stress traction read, respectively,

$$p_3 = \pm \left( t_{23} + \frac{1}{2} \mu_{22,1} \right), \quad q_1 = \pm \mu_{21}, \quad q_2 = 0. \quad (6)$$

The conditions of dynamic equilibrium of forces and moments read (Koiter,  
 1964, Eqs.(2.7) and (2.9))

$$\sigma_{13,1} + \sigma_{23,2} + \tau_{13,1} + \tau_{23,2} = \rho \ddot{u}_3, \quad (7a)$$

$$\mu_{11,1} + \mu_{21,2} + 2\tau_{23} = J \ddot{\varphi}_1, \quad (7b)$$

$$\mu_{12,1} + \mu_{22,2} - 2\tau_{13} = J \ddot{\varphi}_2, \quad (7c)$$

109 where  $\rho$  is the mass density and  $J$  is the rotational inertia. Within the framework  
 110 of linear deformation, the total strain  $\boldsymbol{\varepsilon}$  and the curvature  $\boldsymbol{\chi}$  are connected to  
 111 the stress and to the couple stress through the isotropic constitutive relations

$$\boldsymbol{\sigma} = 2G\boldsymbol{\varepsilon} + \Lambda(\text{tr } \boldsymbol{\varepsilon})\mathbf{1}, \quad \boldsymbol{\mu} = 2G\ell^2 (\boldsymbol{\chi}^T + \eta\boldsymbol{\chi}) \quad (8)$$

112 where  $\Lambda$  and  $G > 0$  take up the role of Lamé moduli,  $\mathbf{1}$  is the identity tensor,  $\ell >$   
 113  $0$  is a characteristic length and  $-1 < \eta < 1$  is a dimensionless number similar to  
 114 Poisson's ratio. We observe that the contribution of  $\Lambda$  is immaterial for antiplane

115 deformations, cf. (Zhang et al., 1998, Eqs.(8-9)). Besides, the second equation  
 116 in (8) differs from (Koiter, 1964, Eqs.(4.7)) by a factor 2, which is incorporated  
 117 in  $\ell$ . The material parameters  $\ell$  and  $\eta$  depend on the microstructure and can be  
 118 connected to the material characteristic length in bending,  $\ell_b$ , and in torsion,  
 119  $\ell_t$ , through

$$\ell_b = \ell/\sqrt{2}, \quad \ell_t = \ell\sqrt{1+\eta}. \quad (9)$$

120 Values of  $\ell_b$  and  $\ell_t$  may be found in Lakes (1986); Nakamura and Lakes (1995)  
 121 and, as an example, for polyurethane foam we have

$$\ell = 0.462 \text{ mm}, \quad \eta = 0.797$$

122 The limiting value  $\eta = -1$  corresponds to a vanishing characteristic length in  
 123 torsion, which is typical of polycrystalline metals. Clearly, the definitions (9)  
 124 show that  $\ell_t = \ell_b$  for  $\eta = -\frac{1}{2}$  and  $\ell_t = \ell = \sqrt{2}\ell_b$  for  $\eta = 0$ , the latter situa-  
 125 tion being the strain gradient effect considered in Zhang et al. (1998). For the  
 126 limiting value  $\eta = 1$ , the constitutive equation (8) provides a symmetric cou-  
 127 ple stress tensor and, consequently, the present theory reduces to the modified  
 128 couple stress theory of elasticity introduced in Yang, Chong, Lam, and Tong  
 129 (2002). Indeed, the simplified couple stress theory involves only the material  
 130 length  $\ell$  for  $\ell_b = \ell_t/2 = \ell/\sqrt{2}$ .

The constitutive equations (8), together with the kinematic relations (1-4),  
 give stress and couple stress in terms of displacement

$$\sigma_{13} = Gu_{3,1}, \quad \sigma_{23} = Gu_{3,2}, \quad (10a)$$

$$\mu_{11} = -\mu_{22} = G\ell^2(1+\eta)u_{3,12}, \quad \mu_{21} = G\ell^2(u_{3,22} - \eta u_{3,11}), \quad (10b)$$

$$\mu_{12} = -G\ell^2(u_{3,11} - \eta u_{3,22}). \quad (10c)$$

131 We observe that the skew-symmetric part  $\boldsymbol{\tau}$  of the total stress tensor  $\boldsymbol{t}$  is deter-  
 132 mined by rotational equilibrium. Indeed, introduction of Eqs.(10) into Eqs.(7b)  
 133 and (7c) yields

$$\tau_{13} = -\frac{1}{2}G\ell^2\Delta u_{3,1} + \frac{J}{4}\ddot{u}_{3,1}, \quad \tau_{23} = -\frac{1}{2}G\ell^2\Delta u_{3,2} + \frac{J}{4}\ddot{u}_{3,2}, \quad (11)$$



134 which correspond to Eqs.(9) of Mishuris et al. (2012). Here,  $\Delta$  denotes the 2-D  
135 Laplace operator.

### 136 3. Time-harmonic analysis

137 It is found expedient to introduce the reference length  $\lambda\ell$  and the refer-  
138 ence time  $T = \ell/c_s$  along with the dimensionless co-ordinates  $(\xi_1, \xi_2, \xi_3) =$   
139  $(\lambda\ell)^{-1}(x_1, x_2, x_3)$  and the dimensionless time  $\tau = t/T$ . Here,  $c_s = \sqrt{G/\rho}$  is the  
140 shear wave speed of classical elastic media and  $\lambda$  is defined in the following. We  
141 consider a shear traction wave applied to the crack faces and zero micropolar  
142 stress

$$p_3(\xi_1, 0^\pm, \tau) = \pm G\tau_0 \exp[\imath(k\xi_1 + \Omega\tau)], \quad q_1(\xi_1, 0^\pm, \tau) = 0, \quad \xi_1 < 0, \quad (12)$$

143 where  $\imath$  is the imaginary unit and  $\Omega = \omega T > 0$  the dimensionless (time) fre-  
144 quency. Here,  $k$  denotes the dimensionless (spatial) wavenumber and it is a  
145 complex number with non-positive imaginary part, i.e.  $\Im(k) \leq 0$ , to warrant  
146 propagation/decay as  $\xi_1 \rightarrow -\infty$ . In fact, the limiting case  $\Im(k) = 0$  corresponds  
147 to a propagating wave with phase velocity

$$c = \frac{\Omega}{k}\lambda. \quad (13)$$

148 When  $\Re(k) \leq 0$ , the applied wave is impinging upon/moving out of the crack-  
149 tip. In the special case  $\Re(k) = 0$ , a harmonic (in time) loading, exponentially  
150 decaying along the crack, is considered. We observe that, in the general case,  
151  $\tau_0 = \tau_0(k, \Omega)$  and this problem may be used as a building block to solve any  
152 harmonic wave propagation problem in a cracked couple stress half-space in  
153 antiplane deformation.

154 Assuming the same time-harmonic variation for the out-of-plane displace-  
155 ment as in the applied wave (12)

$$u_3(\xi_1, \xi_2, \tau) = \ell w(\xi_1, \xi_2) \exp \imath \Omega \tau,$$

156 and substituting Eqs.(10a-11) into (7-7c), we get the metaharmonic PDE Geor-  
157 giadis and Velgaki (2003) for the function  $w$ :

$$\Delta \Delta w - 2(1 - h_0^2 \Omega^2) \lambda^2 \Delta w - 2\Omega^2 \lambda^4 w = 0, \quad (14)$$

158 where  $\Delta w = w_{,11} + w_{,22}$  and we have let the dimensionless parameter Mishuris  
159 et al. (2012)

$$h_0 = \frac{h}{\ell}, \quad \text{with} \quad h = \frac{1}{2} \sqrt{\frac{J}{\rho}}.$$

160 We observe that  $h$  is proportional to the dynamic characteristic length intro-  
161 duced in Shodja et al. (2015). This generalized bi-harmonic equation can be  
162 easily factored

$$(\Delta + \delta^2) (\Delta - 1) w = 0, \quad (15)$$

163 where we have let the positive dimensionless parameter

$$\delta = \frac{1}{\sqrt{2}\Omega} \left[ \sqrt{(1 - h_0^2 \Omega^2)^2 + 2\Omega^2} - 1 + h_0^2 \Omega^2 \right], \quad (16)$$

and, for convenience, we have chosen the scaling factor  $\lambda$  as to have 1 in the  
second factor of Eq.(15)

$$\lambda = \sqrt{\frac{\delta}{\sqrt{2}\Omega}}.$$

164 We observe that  $\lambda$  is a strictly monotonic increasing (decreasing) function of  $\Omega$   
165 inasmuch as  $h_0 \geq h_{0cr} = 1/\sqrt{2}$ , while  $h_0 = h_{0cr}$  lends  $\lambda \equiv h_{0cr}$ . Besides, in the  
166 static limit  $\Omega = 0$ , we get  $\delta = 0$ ,  $\lambda = h_{0cr}$  and the factorization boils down to

$$\Delta (\Delta - 1) w = 0,$$

167 that recovers the governing equation for the static regime considered in (Radi,  
168 2008, Eq.(10)) and in (Zhang et al., 1998, Eq.(11)). It is worth emphasizing  
169 that the limiting case  $\eta = -1$  lends the Mode III crack problem of classical  
170 linear elasticity in the static regime only.

171 Using Eqs.(1,8,10b, 11) into the first of Eqs.(6), the corresponding loading  
172 conditions (12) becomes

$$(1 - \delta^2)w_{,2} - [(2 + \eta)w_{,11} + w_{,22}]_{,2} = 2\lambda^3 \tau_0 \exp \imath k \xi_1, \quad \xi_1 < 0, \xi_2 = 0^+. \quad (17)$$

Besides, the skew-symmetric character of Mode III requires

$$w(\xi_1, 0) = 0, \quad \xi_1 > 0, \quad (18a)$$

$$q_1(\xi_1, 0) = 0, \quad \xi_1 > 0. \quad (18b)$$

Therefore, the condition of zero micropolar traction  $q_1(\xi_1, 0) = 0$  stands along the whole crack line and, in light of Eqs.(6,10b), it gives

$$w_{,22} - \eta w_{,11} = 0, \quad \xi_2 = 0. \quad (19)$$

We note that the material parameter  $\eta$  only appears in the boundary conditions (17) and (19).

### 3.1. Edge-waves for antiplane deformation

Planar shear waves travelling in the bulk of the material have been considered in (Mishuris et al., 2012, §2.1). Here, similarly to Ottosen et al. (2000); Georgiadis and Velgaki (2003), we look at edge-wave solutions

$$u_3(\xi_1, \xi_2, \tau) = \ell W(\xi_2) \exp[i(m\xi_1 + \Omega\tau)],$$

where  $W(\xi_2)$  decays fast enough away from the crack line and we assume  $m$  to be real. Then, Eq.(15) governing harmonic motion for antiplane deformation gives

$$W'''' + (\delta^2 - 2m^2 - 1)W'' + (m^2 + 1)(m^2 - \delta^2)W = 0,$$

which admits the solution

$$W(\xi_2) = C_1 \exp[-\alpha(m)\xi_2] + C_2 \exp[-\beta(m)\xi_2], \quad (20)$$

where

$$\alpha(s) = \sqrt{s^2 - \delta^2}, \quad \beta(s) = \sqrt{s^2 + 1}. \quad (21)$$

The constants  $C_1$  and  $C_2$  are determined imposing homogeneous boundary conditions on the crack surface, which amounts to the vanishing of reduced force and couple stress traction at  $\xi_2 = 0$ ,

$$\begin{cases} W'(0) + \frac{1}{1-\delta^2} [(2+\eta)m^2W'(0) - W''''(0)] = 0, \\ W'''(0) + \eta m^2 W(0) = 0. \end{cases} \quad (22)$$

Plugging Eq.(20) into the boundary conditions (22) yields the following linear system for the constants  $C_1$  and  $C_2$

$$\begin{cases} \alpha(m) [(\eta+1)m^2 + 1] C_1 + \beta(m) [(\eta+1)m^2 - \delta^2] C_2 = 0 \\ [(\eta+1)m^2 - \delta^2] C_1 + [(\eta+1)m^2 + 1] C_2 = 0 \end{cases},$$

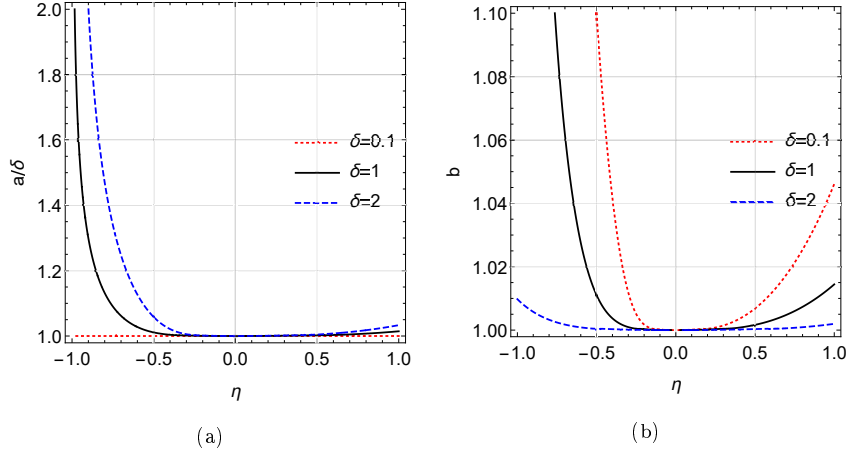


Figure 2: Location of the real root  $a$  (a) of the purely imaginary root  $\iota b$  (b) as a function of  $\eta$  for  $\delta = 0.1$  (red, dotted),  $\delta = 1$  (black, solid) and  $\delta = 2$  (blue, dashed)

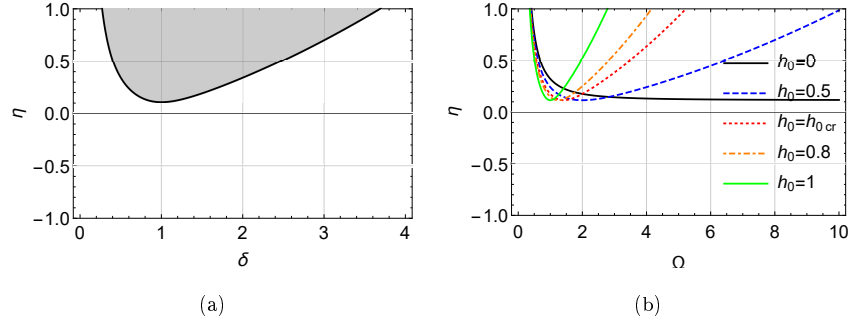


Figure 3: Domain  $(\delta, \eta)$  for the complex root  $s_3$  to sit in the physical Riemann sheet: (a) outside the shaded area  $s_3$  slips through the branch cut out of the physical sheet; (b) role of  $h_0$  on the domain  $(\Omega, \eta)$

183 which admits non-trivial solutions if and only if the following secular equation  
184 is satisfied

$$R(m) = 0, \quad (23)$$

185 where

$$R(s) = \alpha(s) [(\eta + 1)s^2 + 1]^2 - \beta(s) [(\eta + 1)s^2 - \delta^2]^2. \quad (24)$$

186 The function  $R(s)$  is the Rayleigh wave function for antiplane deformation  
187 in couple stress elastic materials. It can be compared with (Freund, 1998,  
188 Eq.(2.5.12)), valid for classical elastic materials. For the selected branch cuts,

189 the function  $R(s)$  is single valued and analytic in the cut  $s$ -plane. In contrast to  
 190 classical elasticity (Freund, 1998, §2.5.2), for the considered range of variation  
 191 of the parameters  $\delta$  and  $\eta$ , Eq.(23) admits *three* complex conjugated pairs of  
 192 order-1 roots, namely two real roots  $s = \pm a$ , two purely imaginary roots  $s = \pm \imath b$   
 193 and the pair of complex roots  $s = \pm s_3$ , which may fall out of the physical Rie-  
 194 mann sheet. The location of the roots  $a$  and  $\imath b$  against the parameters  $\eta$  and  $\delta$  is  
 195 presented in Fig.2. There, it can be observed that  $a \geq \delta$ ,  $b \geq 1$  and yet they sit  
 196 very close to the branch points, especially for  $\eta > -1/2$ . In particular, equality  
 197 holds for  $\eta = 0$ , for which value roots become of order 1/2. In the static case it  
 198 is  $\delta = 0$  and we have  $a = 0$  of order 1.

199 The pair of imaginary roots  $\pm \imath b$  is here connected to the strain-gradient  
 200 effect. In general, it is associated to a fourth-order governing equation and it  
 201 accounts for the edge-effect in shell theories Kaplunov and Nobili (2017) or for  
 202 evanescent modes in supported plates Nobili, Radi, and Lanzoni (2017). The  
 203 additional pair of complex roots,  $\pm s_3$ , exists in the physical Riemann sheet in  
 204 the domain  $(\delta, \eta)$  plotted in Fig.3.

205 The real root  $a > 0$  of the dispersion relation (23) provides the Rayleigh  
 206 wave speed  $c_R$  according to Eq.(13)

$$\frac{c_R}{c_s} = \frac{1}{a} \sqrt{\frac{\Omega \delta}{\sqrt{2}}} = \frac{\sqrt{\sqrt{(1 - h_0^2 \Omega^2)^2 + 2\Omega^2} - 1 + h_0^2 \Omega^2}}{\sqrt{2}a}. \quad (25)$$

207 In the static limit,  $\Omega \rightarrow 0^+$ , we have  $a \sim \delta \rightarrow \Omega/\sqrt{2}$ , whence  $c_R \rightarrow c_s$  and edge-  
 208 waves collapse into classical shear waves. In the special case  $\eta = 0$ , the roots  $a$   
 209 and  $\imath b$  are located on the branch points  $\delta$  and  $\imath$ , respectively, while  $s_3$  falls out  
 210 the physical sheet. In this case, replacing  $a$  with  $\delta$  in Eq.(25) and using Eq.(16)  
 211 gives the speed  $\tilde{c}$  of bulk shear waves (cf. (Mishuris et al., 2012, Eq.(14)))

$$\frac{\tilde{c}}{c_s} = \frac{\sqrt{\sqrt{(1 - h_0^2 \Omega^2)^2 + 2\Omega^2} + 1 - h_0^2 \Omega^2}}{\sqrt{2}}.$$

212 In fact, we have  $\alpha(\delta) = 0 = \beta(\imath)$  and the solution (20) is no longer decaying  
 213 away from the crack line. In the special case  $h_0 = h_{0cr}$  and  $\eta = 0$ , edge-waves  
 214 collapse into non-dispersive shear waves, i.e.  $c_R = \tilde{c} \equiv c_s$ .

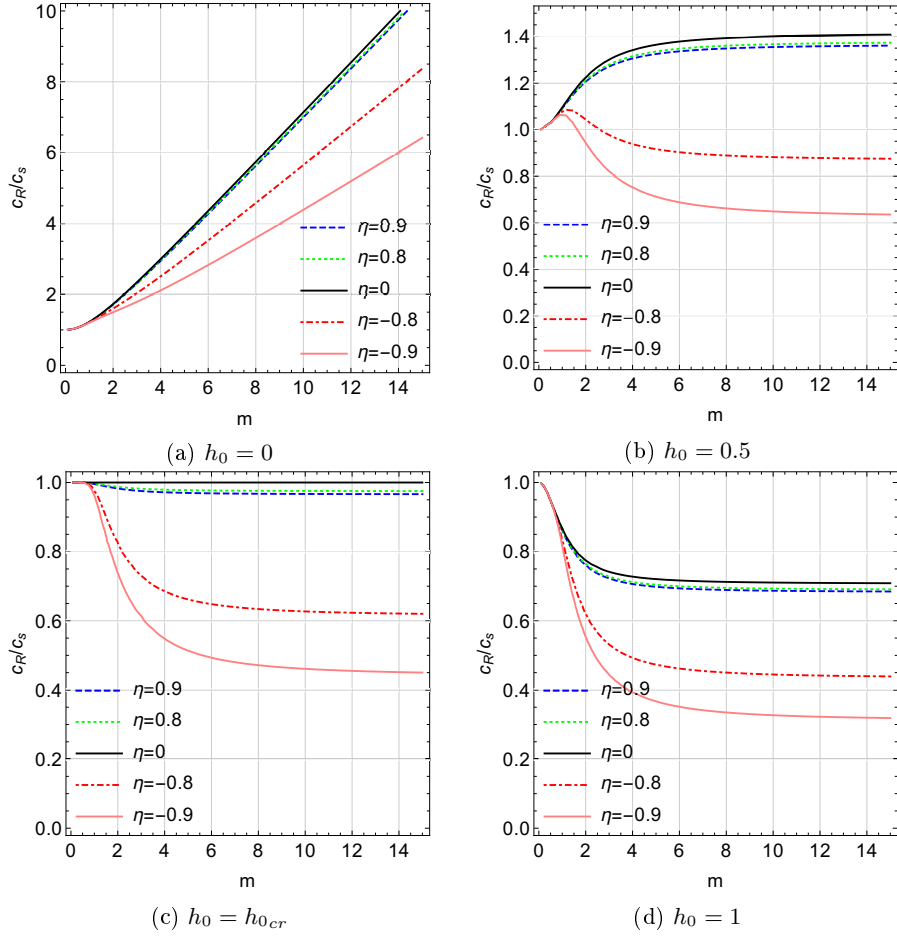


Figure 4: Dispersion curves for the dimensionless Rayleigh wave speed  $c_R/c_s$  (the curve  $\eta = 0$  corresponds to the bulk wave speed  $\tilde{c}/c_s$ )

215 Dispersion curves for the relative edge-wave speed  $c_R/c_s$  for different values  
 216 of the microstructural parameters  $h_0$  and  $\eta$  are plotted in Fig.4. As it is usually  
 217 the case, edge-waves occur at speed slightly below that of bulk waves Destrade,  
 218 Fu, and Nobili (2016). As anticipated, in the static limit, the antiplane edge-  
 219 wave speed  $c_R$  recovers the shear wave speed of classical elastic media  $c_s$ . We ob-  
 220 serve that, in the absence of rotational inertia (i.e.  $h_0 = 0$ ), the edge-wave speed  
 221  $c_R$  grows monotonically with the wavenumber (Fig.4a) and waves are thereby  
 222 dispersive, as already found in Graff and Pao (1967); Ottosen et al. (2000) for  
 223 plane-strain Rayleigh waves. Besides,  $c_R > c_s$ , which is physically unrealistic  
 224 (Shodja et al., 2015). In contrast, for  $h_0 > 0$ , the edge-wave speed quickly  
 225 asymptotes a finite limit and the dispersive character of propagation is really  
 226 restricted to low wavenumbers. Propagation turns perfectly non-dispersive, as  
 227 in classical elastic materials, with speed  $c_R \equiv c_s$ , for  $h_0 = h_{0cr}$  and  $\eta = 0$ , see  
 228 Fig.4c. For  $h_0 > h_{0cr}$  and  $\eta \neq 0$  or for  $h_0 > 0$  and  $\eta$  close enough to  $-1$ , the  
 229 edge-wave speed becomes a decreasing function of wavenumber. This behaviour  
 230 is discussed in Georgiadis and Velgaki (2003), in the context of plane-strain  
 231 Rayleigh wave propagation, with reference to experimental results and lattice  
 232 theories.

Fig.5 superposes dispersion curves for the group velocity  $c_g$

$$\frac{c_g}{c_s} = \frac{\lambda^2}{\frac{dm}{d\Omega}\lambda - m\frac{d\lambda}{d\Omega}},$$

233 over the corresponding dispersion curve for the Rayleigh wave phase velocity  $c_R$ .  
 234 Dispersion is termed *anomalous* when  $c_g > c_R$  and *normal* otherwise (Achen-  
 235 bach, 2012, §6.5). Anomalous dispersion is met for  $h_0 = 0$  at any  $\eta$  and for  
 236  $0 < h_0 < h_{0cr}$  and  $\eta$  close to 1. This condition is related to energy propagating  
 237 faster than the wavelets which build up at the front of the group and slowly  
 238 move to the back until they disappear, see (Gourgiotis et al., 2013, §2) in the  
 239 context of gradient elasticity.

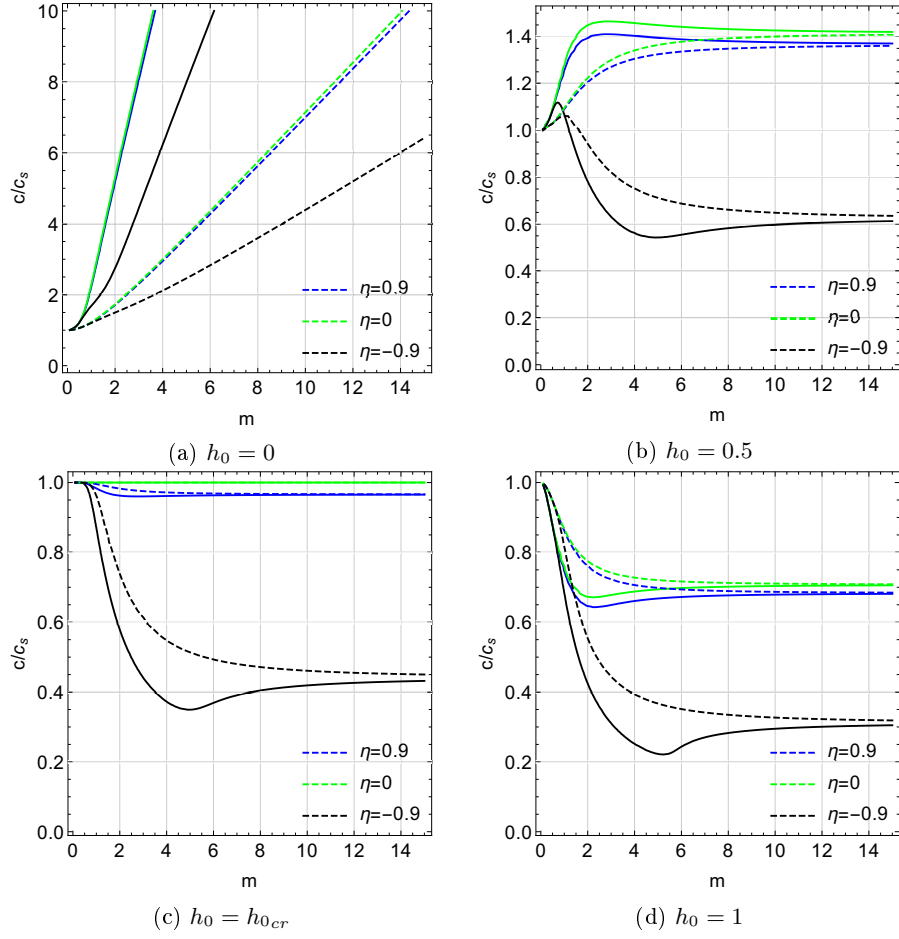


Figure 5: Relative group velocity  $c_g/c_s$  (solid) and Rayleigh wave speed  $c_R/c_s$  (dashed) as a function of wavenumber (the curve  $\eta = 0$  corresponds to the bulk wave speed  $\tilde{c}/c_s$ )



#### 240 4. Analysis in the frequency domain

241 We adopt Fourier transforms to recast the problem in the frequency domain.  
 242 Owing to the skew-symmetry of the problem, only either half-plane, say  $\xi_2 > 0$ ,  
 243 needs to be considered. The full-range Fourier transform along  $\xi_1$  is defined as  
 244 Noble (1958); Roos (1969)

$$\bar{w}(s, \xi_2) = \int_{-\infty}^{\infty} w(\xi_1, \xi_2) \exp(\imath \xi_1 s) d\xi_1,$$

245 while Fourier inversion formula gives

$$w(\xi_1, \xi_2) = (2\pi)^{-1} \int_{\mathcal{L}} \bar{w}(s, \xi_2) \exp(-\imath \xi_1 s) ds.$$

246 In the inverse transform, the integration path  $\mathcal{L}$  is obtained by deformation of  
 247 the real interval, as described in the following. The complex plane  $\mathbb{C}$  is split  
 248 into two domains,  $\mathbb{C} = \mathcal{D}^+ \cup \mathcal{D}^-$ , respectively lying on and above and on and  
 249 below the integration path  $\mathcal{L}$ .

Let us define the half-range Fourier transforms

$$\bar{w}^-(s) = \int_{-\infty}^0 w(\xi_1, 0) \exp(\imath \xi_1 s) d\xi_1, \quad \bar{p}_3^+(s) = \int_0^{\infty} p_3(\xi_1, 0) \exp(\imath \xi_1 s) d\xi_1.$$

Taking the full-range Fourier transform of Eq.(15) gives

$$\bar{w}_{,2222} - (2s^2 + 1 - \delta^2)\bar{w}_{,22} + (s^2 + 1)(s^2 - \delta^2)\bar{w} = 0,$$

250 which admits the solution (20)

$$\bar{w}(s, \xi_2) = C_1 \exp[-\alpha(s)\xi_2] + C_2 \exp[-\beta(s)\xi_2], \quad (26)$$

251 where  $C_1$  and  $C_2$  are complex-valued functions of  $s$ .

252 Here  $\alpha(s)$  and  $\beta(s)$  are defined as in (21) but now  $s$  is generally complex  
 253 and we need to specify the branch in the square root so that (26) is bounded as  
 254  $\xi_2 \rightarrow +\infty$ . The branch cuts for  $\alpha(s)$ , denoted by  $\mathcal{K}^\mp$ , are straight and connect,  
 255 respectively, the branch points  $s = \pm\delta$  to  $\infty$  in the direction  $\mp(\delta + \imath)$  and thereby  
 256 they pass through  $s = \mp\imath$ , as shown in Fig.6. They may be parametrized as

$$\mathcal{K}^\mp = \{s(t) = \pm\delta \mp (\delta + \imath)t, \quad t > 0\}. \quad (27)$$

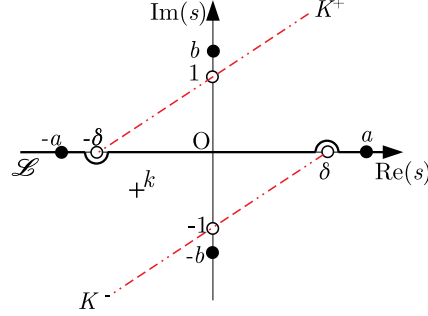


Figure 6: Branch cuts  $\mathcal{K}^\pm$  (red dash-double dot lines), zeros (black dots), branch points (circles), applied traction wavenumber (cross) and integration path  $\mathcal{L}$  (solid curve) in the complex plane  $\mathbb{C} = \mathcal{D}^+ \cup \mathcal{D}^-$ . The domains  $\mathcal{D}^\pm$  stand on and above (under) the integration path  $\mathcal{L}$ , respectively

257 In likewise fashion, the branch cuts for  $\beta(s)$  rest inside  $\mathcal{K}^\mp$  and connect the  
 258 branch points  $s = \pm i$  to  $\mp(\delta + i)\infty$ , i.e. they have the parametrization (27)  
 259 with  $t > 1$ . Square root is made definite by letting  $\alpha(s)$  and  $\beta(s)$  tend to  $|s|$   
 260 as  $s \rightarrow \infty$  along the real axis (see (Noble, 1958, p.10)). With such definitions,  
 261 the square roots in  $\alpha(s)$  and  $\beta(s)$  are defined so as to have positive or zero real  
 262 part (respectively decaying and propagating solutions) when  $s$  is real. Indeed,  
 263 for  $s = s_1 \in \mathbb{R}$ , it is

$$\alpha(s_1) = \begin{cases} i\sqrt{\delta^2 - s_1^2}, & |s_1| < \delta \\ \sqrt{s_1^2 - \delta^2}, & s_1 \geq \delta \end{cases}, \quad \beta(s_1) = \sqrt{s_1^2 + 1}. \quad (28)$$

264 The full-range transform of the reduced traction vector at the l.h.s of Eq.(17)  
 265 is

$$\bar{p}_3(s, \xi_2) = \frac{G}{2\lambda^3} [((2 + \eta)s^2 + 1 - \delta^2) \bar{w}_{,2} - \bar{w}_{,222}]. \quad (29)$$

266 The minus half-range Fourier transform of the first boundary condition (12)  
 267 reads

$$\bar{p}_3^-(s, 0) = -i \frac{G\tau_0}{s + k}, \quad (30)$$

268 and the plus transform of Eq.(18a) lends

$$\bar{w}^+(s, 0) = 0, \quad (31)$$

269 while the full-range transform of Eq.(19) gives

$$\bar{w}_{,22}(s, 0) + \eta s^2 \bar{w}(s, 0) = 0. \quad (32)$$

270 Plugging the solution (26) into Eq.(32) gives a connection between  $C_1$  and  $C_2$

$$C_1 = -\frac{(\eta + 1)s^2 + 1}{(\eta + 1)s^2 - \delta^2} C_2. \quad (33)$$

271 Thus, making use of the general solution (26) and of the connection (33), we  
272 find for the full-range Fourier transform of the traction vector (29)

$$\frac{G(1 + \delta^2)}{2\lambda^3 [(\eta + 1)s^2 - \delta^2]} K(s) C_2 = \bar{p}_3^+(s, 0) - i \frac{G\tau_0}{s + k}, \quad (34)$$

273 where

$$K(s) = (1 + \delta^2)^{-1} R(s), \quad (35)$$

274 and  $R(s)$  is the Rayleigh function introduced in Eq.(24). The kernel function  
275  $K(s)$  is even and it obeys the reflection principle

$$K(s^*) = K(s)^*, \quad (36)$$

276 where a superscript asterisk denotes complex conjugation, i.e.  $s^* = \Re(s) - i\Im(s)$ .

277 As a consequence,  $K(s)$  is real-valued on the real axis.

278 In light of Eqs.(26,31) and (33), we get for the displacement  $\bar{w}(s, 0)$

$$-\frac{1 + \delta^2}{(\eta + 1)s^2 - \delta^2} C_2 = \bar{w}^-(s, 0). \quad (37)$$

279 Solving Eq.(37) for  $C_2$  and substituting into Eq.(34) yields the inhomogeneous

280 Wiener-Hopf functional equation

$$G^{-1} \bar{p}_3^+(s, 0) = -\frac{1}{2\lambda^3} K(s) \bar{w}^-(s, 0) + i \frac{\tau_0}{s + k}. \quad (38)$$

#### 281 4.1. Asymptotic behaviour

The asymptotic behaviour of the out of plane reduced traction and displacement at the crack tip is expected to be the same as what is obtained in the

stationary crack problem under quasi-static loading, respectively (Radi, 2008, Eq.(39) and (40))

$$\begin{aligned} p_3(\xi_1, 0) &= O\left(\xi_1^{-3/2}\right), & \text{as } \xi_1 \rightarrow 0^+, \\ w(\xi_1, 0) &= O\left((-\xi_1)^{3/2}\right), & \text{as } \xi_1 \rightarrow 0^-. \end{aligned}$$

Consequently, the Tauberian theorem for the Fourier transform gives Roos (1969)

$$\bar{p}_3^+(s, 0) = O\left(s^{1/2}\right), \quad \text{and} \quad \bar{w}^-(s, 0) = O\left(s^{-5/2}\right), \quad \text{as } |s| \rightarrow \infty. \quad (39)$$

#### 4.2. Radiation condition

As discussed in (Noble, 1958, §1.5), application of the W-H technique requires a strip of regularity, which is warranted when a small imaginary part for  $\delta$  is assumed such that  $\delta^2 = \delta_1^2 - \epsilon\delta_1$ . Nonetheless, the limiting situation  $\epsilon = 0$  is still accessible provided that Sommerfeld's radiation condition is enforced. This demands that elastic waves transfer energy *from* the loading zone *to* infinity and not vice versa. In particular, along the crack surface, energy is carried away by Rayleigh waves, travelling in the negative  $\xi_1$ -direction with the speed  $c_R$  defined in Eq.(25). Accordingly, proceeding as in Sec.3.1, we have

$$w(\xi_1, 0) = A \exp(\imath a \xi_1) + O(\xi_1^{-\rho}), \quad \text{as } \xi_1 \rightarrow -\infty,$$

where  $A$  is a constant and  $\rho > 0$  warrants decay. The corresponding minus Fourier transform can be split as

$$\bar{w}^-(s, 0) = \int_{-\infty}^{-M} + \int_{-M}^0 w(\xi_1, 0) \exp(\imath s \xi_1) d\xi_1,$$

for any large positive constant  $M$ . We observe that the second integral is an entire function, for it has no singular points in the complex plane. Consequently, all singular points of the function  $\bar{w}^-(s, 0)$  come with the first integral

$$\int_{-\infty}^{-M} \exp[-\imath(s+a)\xi_1] d\xi_1 = \frac{\imath}{s+a} \exp[\imath M(s+a)],$$

which indeed brings the singular point  $s = -a$ . Therefore, it follows that

$$\bar{w}^-(s, 0) = (s+a)^{-1}, \quad \text{as } s \rightarrow -a. \quad (40)$$

289 Along every other direction, different from the negative  $\xi_1$ -axis, Sommer-  
 290 feld's radiation condition for the governing equation (14) requires, in polar co-  
 291 ordinates  $(r, \vartheta)$ ,  $r = (\xi_1^2 + \xi_2^2)^{1/2}$ , (Noble, 1958, §1.5)

$$\frac{\partial w}{\partial r} + \imath \delta w = o\left(\frac{1}{\sqrt{r}}\right), \quad \text{as } r \rightarrow \infty \quad (\vartheta \neq \pm\pi), \quad (41)$$

292 uniformly in  $\vartheta$ . Such behaviour should be recovered by the present solution,  
 293 although the field equation (12) is not of the classical Helmholtz type Geor-  
 294 giadis and Vardoulakis (1998). Condition (41) is compatible with the following  
 295 asymptotic behaviour for the displacement along radial lines

$$w(r, \vartheta) = O\left(r^{-1/2} \exp(-\imath r \delta)\right), \quad \text{as } r \rightarrow \infty \quad (\vartheta \neq \pm\pi),$$

296 and in particular, for  $\vartheta = \pi/2$ , the  $\xi_2$ -axis is considered

$$w(0, \xi_2) = O\left(\xi_2^{-1/2} \exp(-\imath \xi_2 \delta)\right), \quad \text{as } \xi_2 \rightarrow \infty. \quad (42)$$

Taking the inverse transform of (26) and using Eqs.(33,37) we have

$$w(0, \xi_2) = \frac{1}{2\pi(\delta^2 + 1)} \int_{\mathcal{L}} \left\{ (\delta^2 - (\eta + 1)s^2) \exp[-\xi_2 \beta(s)] \right. \\ \left. + ((\eta + 1)s^2 + 1) \exp[-\xi_2 \alpha(s)] \right\} \bar{w}^-(s, 0) ds, \quad (43)$$

and, in consideration of (28), the limit as  $\xi_2 \rightarrow \infty$  is given by

$$w(0, \xi_2) \rightarrow \frac{1}{2\pi(\delta^2 + 1)} \int_{-\delta}^{\delta} ((\eta + 1)s^2 + 1) \exp[-\xi_2 \alpha(s)] \bar{w}^-(s, 0) ds.$$

Then, by the method of stationary phase Bleistein and Handelsman (1975), it  
 can be shown that  $w(0, \xi_2)$  behaves as in Eq.(42). We observe that, setting  
 $\xi_2 = 0$  in Eq.(43), one gets

$$w(0, 0) = \frac{1}{2\pi(\delta^2 + 1)} \int_{\mathcal{L}} \bar{w}^-(s, 0) ds = 0,$$

297 the last equality being obtained by Jordan's lemma.

## 298 5. Full-field solution by the Wiener-Hopf method

In the present section the Wiener-Hopf analytic continuation technique No-  
 ble (1958); Roos (1969); Freund (1998) is used to obtain the full-field solution

for a semi-infinite crack in a half-space subject to a reduced traction shear wave applied to the crack surfaces. For the application of the Wiener-Hopf (W-H) method, knowledge of the number and of the location of all roots of the kernel function  $K(s)$ , as defined in Eq.(35), is demanded Noble (1958). Besides, the behaviour of  $K(s)$  as  $|s| \rightarrow \infty$  is required

$$K(s) = c|s|^3 + O(|s|), \quad \text{as } |s| \rightarrow \infty,$$

where  $c = \frac{1}{2}(\eta + 1)(3 - \eta)$ . With this knowledge, the function  $K(s)$  can be factorized into the product of two functions,  $K^\pm(s)$ , analytic in the corresponding domain  $\mathcal{D}^\pm$  (Fig.6). Indeed, let us introduce the function

$$F(s) = \frac{\alpha(s)K(s)}{c(s^2 - a^2)(s^2 + b^2)} \frac{s^2 - s_0^2}{s^2 - s_3^2}, \quad (44)$$

where  $s_0$  is a special point defined in Eq.(A.4). The choice of  $\beta(s)$  in place of  $\alpha(s)$  at the numerator of  $F(s)$  is equally possible but it prevents considering the special cases  $\eta = 0$  and  $\delta = 0$  within the general framework. Indeed, for  $\eta = 0$ , the roots  $\pm a$  and  $\pm b$  coincide with the branch points  $\pm \delta$  and  $\pm \iota$ , respectively, and they become of order 1/2. Similarly, for  $\delta = 0$ , the pair of simple roots  $\pm a$  collapse into the *simple* root  $a = 0$ .

The function  $F(s)$  is even, satisfies the reflection principle (36), and it tends to 1 as  $|s| \rightarrow \infty$ . Besides, it has neither roots nor poles in the cut physical sheet, although it exhibits two branch cuts with the parametrized representation

$$\mathcal{F}^\pm = \{\mp \delta \pm (\delta + \iota)t, \quad t \in [0, 1]\} \subset \mathcal{K}^\pm. \quad (45)$$

Consequently, it admits the product decomposition  $F(s) = F^+(s)F^-(s)$ , where the functions  $F^\pm(s)$  are analytic in the domains  $\mathcal{D}^\pm$ , respectively. Since  $F(s)$  is even, we can assume, without loss of generality,

$$F^\pm(-s) = F^\mp(s). \quad (46)$$

Details of the factorization may be found in Appendix A.

Once the factorization has been accomplished, Eq.(44) provides

$$K^\pm(s) = \sqrt{c} \frac{(s \mp a)(s \pm \iota b)}{\alpha^\pm(s)} \frac{s \pm s_3}{s \pm s_0} F^\pm(s), \quad (47)$$

316 so that  $K^\pm(-s) = K^\mp(s)$  and we have the leading term asymptotics

$$K^\pm(s) = \sqrt{c} \exp(\pm i\pi/4) s^{3/2}, \quad \text{as } |s| \rightarrow \infty,$$

in the relevant analyticity region. Here, the functions  $\alpha(s)$  and  $\beta(s)$  are factorized into the product of two functions, named plus and minus, respectively analytic in  $\mathcal{D}^+$  and  $\mathcal{D}^-$ , namely

$$\alpha^\pm(s) = e^{\mp i\pi/4} \sqrt{s \mp \delta}, \quad \beta^\pm(s) = e^{\mp i\pi/4} \sqrt{s \pm i}.$$

317 The factor  $e^{\mp i\pi/4}$  warrants that we have  $\alpha^\pm(-s) = \alpha^\mp(s)$  and  $\beta^\pm(-s) = \beta^\mp(s)$ .

318 The W-H equation (38) becomes

$$\frac{p_3^+(s, 0)}{GK^+(s)} = -\frac{1}{2\lambda^3} K^-(s) \bar{w}^-(s, 0) + i \frac{\tau_0}{(s+k)K^+(s)}. \quad (48)$$

Therefore, in light of (39), both the l.h.s. and the first term at the r.h.s. in Eq.(48) behave as  $O(s^{-1})$  as  $|s| \rightarrow \infty$ , whereas the last term at the r.h.s. behave as  $O(s^{-5/2})$ . This last term may be easily split into the sum of a plus and a minus function (indeed  $-k$  is not a zero for  $K^+(s)$ )

$$\begin{aligned} \frac{p_3^+(s, 0)}{GK^+(s)} - i \frac{\tau_0}{s+k} \left[ \frac{1}{K^+(s)} - \frac{1}{K^+(-k)} \right] \\ = -\frac{1}{2\lambda^3} K^-(s) \bar{w}^-(s, 0) + i \frac{\tau_0}{(s+k)K^+(-k)}, \end{aligned}$$

319 so thus the l.h.s. is a plus function while the r.h.s is a minus function. Therefore,  
 320 either hand is an entire function in the relevant domain and, in consideration  
 321 of the common strip of analyticity existing between the two (which is really the  
 322 line  $\mathcal{L}$ ), analytic continuation warrants they are the *same* entire function  $E(s)$ .  
 323 Determination of  $E(s)$  hinges on the extended form of Liouville's theorem and  
 324 on the asymptotic behaviour expected at infinity, see Sec.4.1. Consequently,  
 325  $E(s) \equiv 0$  and

$$\bar{w}^-(s, 0) = 2i \frac{\lambda^3}{K^-(k)} \frac{\tau_0}{(s+k)K^-(s)}, \quad (49)$$

326 whose single real pole, in consideration of the definition (47), matches the form  
 327 (40) and thereby satisfies Sommerfeld's radiation condition.

For the plus transform of the reduced traction we have

$$\bar{p}_3^+(s, 0) = \imath G \frac{\tau_0}{s + k} \left[ 1 - \frac{K^+(s)}{K^-(k)} \right],$$

328 and the corresponding full-range Fourier transform, evaluated on the crack line,  
329 easily follows from Eq.(30)

$$\bar{p}_3(s, 0) = -\imath G \frac{\tau_0}{s + k} \frac{K^+(s)}{K^-(k)}. \quad (50)$$

## 330 6. Results

### 331 6.1. Representation of displacement

The inverse Fourier transform of Eq.(49) gives the displacement along the crack line

$$w(\xi_1, 0, \tau) = \imath \lambda^3 \tau_0 \frac{\exp \imath \Omega \tau}{\pi K^-(k)} \int_{\mathcal{L}} \frac{\exp(-\imath s \xi_1)}{(s + k) K^-(s)} ds.$$

Ahead of the crack tip, displacement can be conveniently determined closing the integration path  $\mathcal{L}$  around the top branch cut,  $\mathcal{K}^+$ , and adding the contribution of the poles  $s = -k, -a$  and  $s = \imath b$ , namely

$$\begin{aligned} w(\xi_1, 0, \tau) = & -2\lambda^3 \tau_0 \frac{\exp \imath \Omega \tau}{K^-(k)} \left[ \frac{1}{2\pi \imath} \int_{\mathcal{K}^+} \frac{\exp(-\imath s \xi_1)}{(s + k) K^-(s)} ds + \frac{\exp(\imath k \xi_1)}{K^+(k)} \right. \\ & \left. - \frac{\exp(\imath a \xi_1)}{k - a} \frac{\alpha^+(a)}{\sqrt{c}(a + \imath b) F^+(a)} \frac{a + s_0}{a + s_3} + \frac{\exp(b \xi_1)}{k + \imath b} \frac{\alpha^-(\imath b)}{\sqrt{c}(a + \imath b) F^-(\imath b)} \frac{\imath b - s_0}{\imath b - s_3} \right], \\ & \xi_1 < 0. \end{aligned}$$

We remark that simple poles represent travelling waves. Indeed, the second term in square brackets provides the displacement wave entrained by the traction wave applied at the crack faces, Fig.7a, while the third term brings *outgoing* Rayleigh waves, reflected by the crack-tip. The last term is remarkable in that it represents waves that decay exponentially for  $\xi_1 < 0$  and yet propagate along the  $\xi_2$  direction, Fig.7c. To see this, we note that  $\alpha(\imath b) = -\imath \sqrt{b^2 + \delta^2}$  and  $\beta(\imath b) = -\imath \sqrt{b^2 - 1}$ , whence a pair of waves arises with speed

$$\frac{c_{b1}}{c_s} = \frac{\Omega}{\sqrt{b^2 + \delta^2}} \lambda, \quad \text{and} \quad \frac{c_{b2}}{c_s} = \frac{\Omega}{\sqrt{b^2 - 1}} \lambda.$$



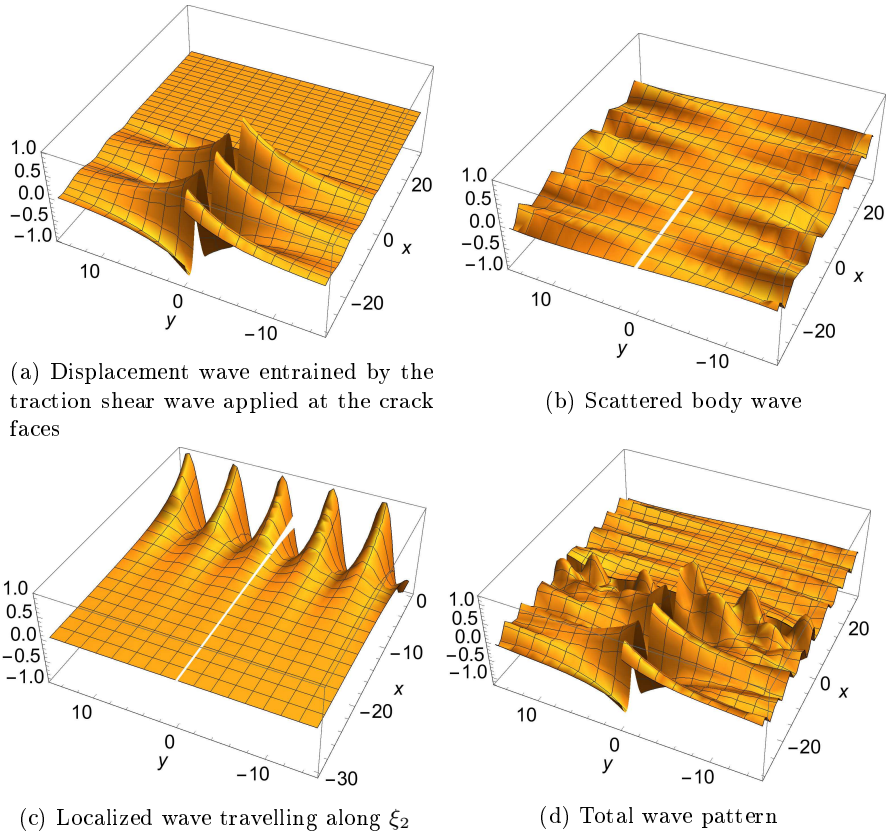


Figure 7: Schematic representation of the wave pattern for  $k < -a$  (each wave is scaled as to improve clarity and only one wave is considered for each contribution; reflected Rayleigh waves are disregarded)

332 Such waves may be put to great advantage in non-destructive material testing  
 333 for they are highly localized along  $\xi_1$  in correspondence of the crack-tip location.  
 334 Furthermore, we observe that unlike  $c_{b1} < c_R \leq c_s$ ,  $c_{b2}$  may be very large and  
 335 greater than the Rayleigh wave speed. The possibility of surface waves moving  
 336 at super-Rayleigh speed in couple-stress materials has been pointed out in Graff  
 337 and Pao (1967) and discussed in Ottosen et al. (2000); Georgiadis and Velgaki  
 338 (2003), in the context of plane strain. Interestingly, we note that for  $\eta = 0$ ,  
 339  $s = -a$  and  $s = ib$  are no longer poles. The first term in square brackets  
 340 represents non-planar body waves, moving with speed  $\tilde{c}$  along the crack line  
 341 and away from the crack-tip, Fig.7b.

342 It's interesting to observe that unboundedness (resonance) occurs only for  
 343  $k = -a$ , that is when the reduced traction shear wave is associated with Rayleigh  
 344 edge-waves being fed *into* the crack-tip. Indeed, when  $k = a$  and Rayleigh waves  
 345 move *out* of the crack-tip, the second and the third term in square brackets  
 346 combine into a bounded term.

347 We now consider the pole  $s = -k$  in the context of the full-field solution  
 348 (43). Eq.(28) shows that the real interval  $|k| < \delta$  is associated with a decaying  
 349 and a propagating wave along  $\xi_2$ , the latter with speed  $c \geq c_R$  greater than  
 350 Rayleigh. Indeed, this result corresponds to a super-Rayleigh loading condition.  
 351 The condition of exponential loading,  $k = ik_2$ ,  $-1 < k_2 < 0$ , still brings a pair  
 352 of waves along  $\xi_2$ , one decaying and the other propagating, yet the latter moves  
 353 with sub-Rayleigh speed  $\Omega\lambda c_s(k_2^2 + \delta^2)^{-1/2}$ . However, when decay is strong  
 354 enough along  $\xi_1$ , i.e.  $k_2 < -1$ , the decaying wave turns propagating along  $\xi_2$   
 355 with speed  $\Omega\lambda c_s/\sqrt{k_2^2 - 1}$ , which generally exceeds  $c_R$ .

356 By Jordan's lemma (Roos, 1969, §1.5), the displacement  $w(\xi_1, 0)$  vanishes  
 357 beyond the crack tip, in agreement with the boundary condition (18a). The full  
 358 displacement field beyond the crack-tip is obtained from Eq.(43) and closing  
 359 the integration path around  $\mathcal{K}^-$ . Then, only body waves moving with speed  $\tilde{c}$   
 360 along the crack line and away from the crack-tip appear. It is concluded that  
 361 the crack tip acts as a scatterer of the applied traction shear wave, Fig.7d.

362 Fig.8 shows the displacement along the crack line for two different values of

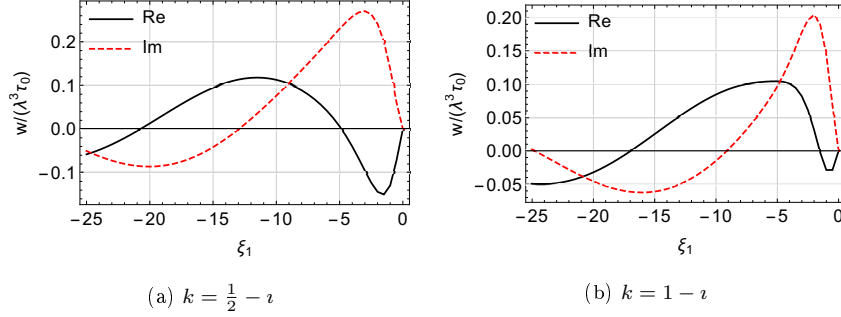


Figure 8: Dimensionless displacement  $w/(\lambda^3\tau_0)$  ahead of the crack tip for  $\delta = 0.2$  and  $\eta = 0.797$

the traction shear wave wavenumber  $k$ .

## 6.2. Representation of stresses

The full-range Fourier transform of the symmetric and of the skew-symmetric shear stress along the crack line read

$$\bar{\sigma}_{23}(s, 0) = -\frac{G}{\lambda(1 + \delta^2)} \{ [(1 + \eta)s^2 + 1]\alpha(s) - [(1 + \eta)s^2 - \delta^2]\beta(s) \} \bar{w}^-(s, 0), \quad (51)$$

and

$$\bar{t}_{23}(s, 0) = -\frac{G}{2\lambda^3(1 + \delta^2)} \{ [(1 + \eta)s^2 + 1]\alpha(s) + \delta^2[(1 + \eta)s^2 - \delta^2]\beta(s) \} \bar{w}^-(s, 0). \quad (52)$$

The Fourier transform of the skew-symmetric shear stress,  $\bar{\tau}_{23}(\xi_1, 0)$ , is then obtained subtracting Eq.(51) from (52). The Fourier transform of the couple stress is given by

$$\bar{\mu}_{22}(s, 0) = i\lambda^{-1}\ell(1 + \eta)s \bar{\sigma}_{23}(s, 0). \quad (53)$$

It is important to observe that  $\bar{\sigma}_{23}(s, 0)$ ,  $\bar{t}_{23}(s, 0)$  and  $\bar{\mu}_{22}(s, 0)$  are not plus functions, although they are analytic in the half-plane  $\Im(s) > b$ . This analyticity property warrants that the Tauberian theorems may be applied in the asymptotic analysis of Sec.6.3. In fact, stresses feature in  $\mathcal{D}^+$  the branch cut  $\mathcal{F}^+$ , coming from  $F^-(s)$ , alongside the simple poles  $s = -a$ ,  $ib$  and  $s = -k$ , originating from  $\bar{w}^-(s, 0)$ . Such poles provide travelling wave contributions to the stress field ahead of the crack tip, as described for displacement.

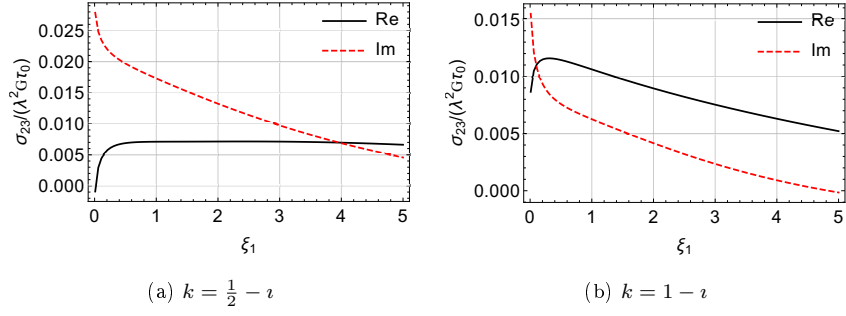


Figure 9: Dimensionless symmetric shear stress  $\sigma_{23}/(\lambda^2 G \tau_0)$ , beyond the crack-tip, for  $\delta = 0.2$  and  $\eta = -0.7$

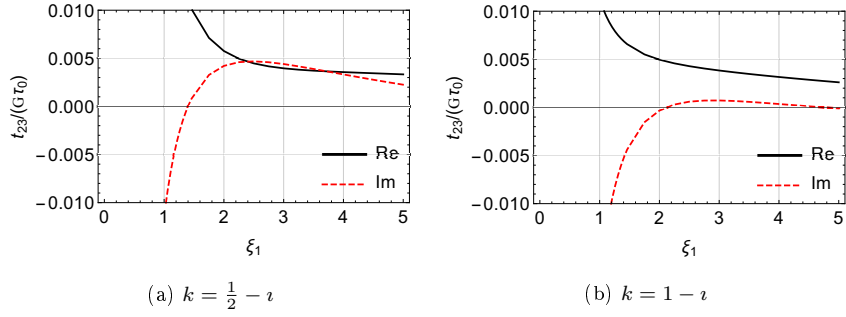


Figure 10: Dimensionless total shear stress  $t_{23}/(G \tau_0)$ , beyond the crack-tip, for  $\delta = 0.2$ ,  $\eta = 0.797$

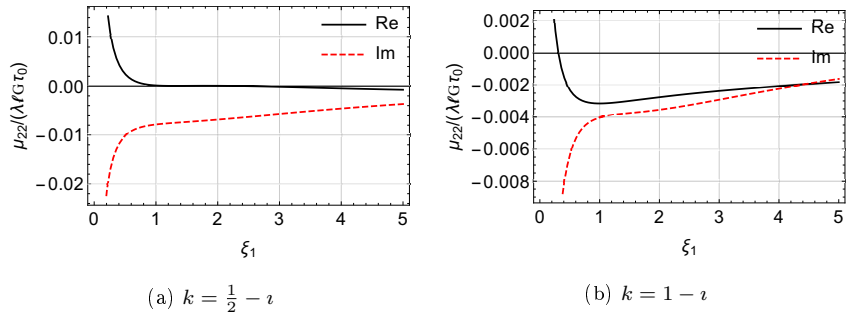


Figure 11: Dimensionless couple stress  $\mu_{22}/(\lambda l G \tau_0)$ , beyond the crack-tip, for  $\delta = 0.2$  and  $\eta = 0.797$

Beyond the crack tip, integration in the inverse Fourier transform for stresses is conveniently carried out closing the integration path  $\mathcal{L}$  around the lower branch cut  $\mathcal{K}^-$ . In particular, such deformation of the integration path is necessary to perform the inverse Fourier transform of Eq.(52), in consideration of the divergent asymptotic behaviour of  $\bar{t}_{23}$  as  $|s| \rightarrow +\infty$ , see Eq.(55). Like for displacement, there are no travelling waves contributing to stress beyond the crack-tip. Indeed, we have the representation formulas for body stress waves

$$\sigma_{23}(\xi_1, 0, \tau) = 2\lambda^2 G\tau_0 \frac{\sqrt{1-\imath\delta}}{\pi(\delta-\imath)K^-(k)} \left[ I_0^{(1)}(\xi_1) - I_1^{(1)}(\xi_1) \right] \exp[\imath(-\delta\xi_1 + \Omega\tau)], \quad (54a)$$

$$t_{23}(\xi_1, 0, \tau) = G\tau_0 \frac{\sqrt{1-\imath\delta}}{\pi(\delta-\imath)K^-(k)} \left[ I_0^{(1)}(\xi_1) + \delta^2 I_1^{(1)}(\xi_1) \right] \exp[\imath(-\delta\xi_1 + \Omega\tau)], \quad (54b)$$

where  $n \in \{1, 2\}$ ,

$$I_{0,1}^{(n)}(\xi_1) = \int_{0,1}^{\infty} f_{0,1}^{(n)}(t) \exp[(\imath\delta - 1)t\xi_1] dt,$$

and

$$f_0^{(n)}(t) = \frac{[(1+\eta)s(t)^2 + 1]^n \alpha^-(s(t))}{[s(t) + k]K^-(s(t))} \sqrt{t}, \quad t > 0,$$

$$f_1^{(n)}(t) = \frac{[(1+\eta)s(t)^2 - \delta^2]^n \beta^-(s(t))}{[s(t) + k]K^-(s(t))} \sqrt{t-1}, \quad t > 1.$$

378 The behaviour of the symmetric and of the total stress is shown in Figs.9 and  
379 10, while couple stress is plotted in Fig.11.

380 From Eq.(50), we write the inversion formula for the reduced total traction

$$p_3(\xi_1, 0, \tau) = -\imath G\tau_0 \frac{\exp \imath\Omega\tau}{2\pi} \int_{\mathcal{L}} \frac{\exp(-\imath s\xi_1)}{s+k} \frac{K^+(s)}{K^-(k)} ds,$$

381 that, ahead of the crack-tip, reduces to the contribution of the pole  $s = -k$   
382 reproducing the applied shear wave. Beyond the crack-tip, we write  $K^+(s) =$   
383  $K(s)/K^-(s)$  and

$$\bar{p}_3(s, 0) = -G \frac{K(s)}{2\lambda^3} \bar{w}^-(s, 0).$$

Upon deforming the integration path around  $\mathcal{K}^-$ , we get the representation formula for reduced traction body waves

$$p_3(\xi_1, 0, \tau) = G\tau_0 \frac{\exp[\imath(-\delta\xi_1 + \Omega\tau)]}{2\pi(1 + \imath\delta)K^-(k)} \left[ I_0^{(2)}(\xi_1) - I_1^{(2)}(\xi_1) \right].$$

### 384 6.3. Dynamic stress intensity factors

385 Eq.(49) immediately provides us with the asymptotics

$$\bar{w}^-(s, 0) = 2\imath^{3/2}\lambda^3\tau_0 \frac{1}{\sqrt{c}K^-(k)} s^{-5/2}, \quad \text{as } |s| \rightarrow \infty,$$

386 valid in the analyticity region  $\mathcal{D}^-$  (we neglect the harmonic term throughout this  
387 Section). Then, the Tauberian theorem (Roos, 1969, §2.14) lends the following  
388 asymptotic representation for the inverse Fourier transform

$$\ell w(x_1, 0) = \text{r.b.m.} + K_{\text{III}}^w(-x_1)^{3/2}, \quad \text{as } x_1 \rightarrow 0^-$$

389 where r.b.m. is an inessential rigid body motion and

$$K_{\text{III}}^w = -16\lambda^{3/2}\tau_0 \frac{1}{3\sqrt{2\pi\ell(1+\eta)(3-\eta)K^-(k)}}.$$

390 Asymptotics for the symmetric, total and couple stress, respectively Eqs.(51,52)  
391 and (53), are similarly obtained

$$\begin{aligned} \bar{\sigma}_{23}(s, 0) &= -\imath^{3/2}\lambda^2 G\tau_0 \frac{1-\eta}{\sqrt{c}K^-(k)} s^{-3/2}, \\ \bar{t}_{23}(s, 0) &= -\imath^{3/2} G\tau_0 \frac{1+\eta}{\sqrt{c}K^-(k)} \sqrt{s}, \quad \text{as } |s| \rightarrow \infty. \\ \bar{\mu}_{22}(s, 0) &= \imath^{1/2}\lambda\ell G\tau_0 \frac{1-\eta^2}{\sqrt{c}K^-(k)} s^{-1/2}, \end{aligned} \quad (55)$$

Then, for the respective inverse Fourier transforms, we infer the asymptotic behaviour

$$\begin{aligned} \sigma_{23}(x_1, 0) &= \Sigma_{23} + K_{\text{III}}^\sigma \sqrt{x_1}, \\ t_{23}(x_1, 0) &= K_{\text{III}}^t x_1^{-3/2}, \quad \text{as } x_1 \rightarrow 0^+, \\ \mu_{22}(x_1, 0) &= K_{\text{III}}^\mu x_1^{-1/2}, \end{aligned}$$

where  $\Sigma_{23}$  can be determined evaluating Eq.(54a) at  $\xi_1 = 0$ . Here, we have let the dynamic stress intensity factors for stresses

$$\begin{aligned} K_{\text{III}}^\sigma &= -4\lambda^{3/2}G\tau_0 \frac{1-\eta}{\sqrt{2\pi\ell(3-\eta)(1+\eta)K^-(k)}}, \\ K_{\text{III}}^t &= -(\lambda\ell)^{3/2}G\tau_0 \sqrt{\frac{1+\eta}{2\pi(3-\eta)}} \frac{1}{K^-(k)}, \\ K_{\text{III}}^\mu &= -2(1-\eta)K_{\text{III}}^t. \end{aligned}$$

Such expressions generalize to the dynamic regime the asymptotic results (Radi, 2008, Eqs.(38)) obtained for static application of the far-field loading  $K_{\text{III}}$ , valid in linear elastic fracture mechanics (LEFM). Indeed, the correction accounts for the important role of frequency of the applied loading on stress concentration (Graff and Pao, 1967). Formal correspondence with LEFM results is met by taking

$$K_{\text{III}} = 2G\tau_0\sqrt{\lambda^3\ell} \frac{1}{K^-(k)}.$$

392 This expression may be explained looking at the far-field behaviour of  $w(r, \vartheta =$   
393  $0)$ ,  $r \rightarrow +\infty$ , which is obtained by investigating the behaviour of  $\bar{w}(s, 0)$  as  
394  $s \rightarrow 0$ . In the general case,  $\bar{w}^-(s, 0)$  behaves like a constant as  $s \rightarrow 0$  and  
395 thereby  $w(r)$  decays as  $r^2$ . In the static limit we have  $\delta = 0$ ,  $\lambda = 2^{-1/2}$  and, for  
396  $k \ll s$ , we get  $K^-(s) \sim \sqrt{K(s)} \sim -\sqrt{\imath s}$  and

$$\bar{w}^-(s, 0) = 2\imath^{3/2} \frac{\lambda^3}{\sqrt{k}} \frac{\tau_0}{s^{3/2}},$$

397 whence, by the Tauberian theorem,

$$\ell w(x_1, 0) = \frac{2K_{\text{III}}}{G} \sqrt{\frac{x_1}{2\pi}},$$

398 which is the far-field behaviour of LEFM (Zhang et al., 1998).

## 399 7. Conclusions

400 Diffraction of reduced traction shear waves applied at the faces of a semi-  
401 infinite rectilinear crack in an elastic half-space with microstructure is con-  
402 sidered. Microstructure is accounted for through the indeterminate theory of

403 couple stress elasticity and motion is restricted to antiplane deformation. The  
 404 full-field solution is obtained in closed form through the Wiener-Hopf technique  
 405 and it may be adopted as a building block for the solution of general wave scat-  
 406 tering problems in a cracked couple-stress half-space. A rather involved wave  
 407 pattern appears, especially when compared to the simple scenario of classical  
 408 elasticity. Indeed we find

- 409 1. entrained waves moving along the crack line with the applied loading  
 410 speed, which may be either decaying away from the crack, in the sub-  
 411 critical regime, or propagating, in the super-critical regime. Transition  
 412 from a sub-critical to a super-critical regime occurs at the Rayleigh speed,  
 413 which is wavenumber dependent (dispersion);
- 414 2. a pair of Rayleigh waves confined to the crack faces and reflected from the  
 415 crack-tip;
- 416 3. a pair of waves highly localized near the crack-tip and moving away from  
 417 it, which may be either decaying and propagating with sub-Rayleigh speed  
 418 or propagating at sub-Rayleigh and super-Rayleigh speed, respectively;
- 419 4. body waves scattered by the crack-tip.

420 Special situations are connected to

- 421 • a loading moving *toward* the crack-tip at Rayleigh speed, because reso-  
 422 nance occurs, i.e. solution is unbounded;
- 423 • an exponentially-decaying loading with harmonic time variation, for the  
 424 associated phase speed is infinite;
- 425 •  $\eta = 0$ , because waves 2 and 3 disappear;
- 426 •  $h_0 = h_{0cr} = 2^{-1/2}$  and  $\eta = 0$ , for then Rayleigh waves become non-  
 427 dispersive and collapse into classical shear waves;
- 428 • the static regime  $\Omega = 0$ , for which Rayleigh waves collapse into classical  
 429 shear waves.



430 Finally, dynamic stress intensity factors are determined for the symmetric  
431 stress, the couple-stress, the total stress and the reduced traction. They gener-  
432 alize to the dynamic regime the corresponding expression already obtained for  
433 the static application of the classical elastic Mode III solution in the far-field.  
434 The correction term brings out the important role of the loading frequency on  
435 the stress intensity factors.

## 436 8. Acknowledgements

437 The authors wish to thank Prof. G. Mishuris for his valuable comments.  
438 AV acknowledges the ERC Grant "Instabilities" for supporting his short stay  
439 in Trento University working on this paper. AN gratefully acknowledges sup-  
440 port from National Group of Mathematical Physics (GNFM-INdAM) through  
441 the Young researchers fellowship programme 2017, Prot. n. U UFMBAZ-  
442 2017/0000259 08/06/2017.

## 443 9. Declaration of interest

444 Authors have no competing interest to declare.

## 445 Appendix A. Factorization of $F(s)$

In the logarithmic factorization, Cauchy theorem is exploited to split  $\ln F(s)$   
into the sum of two functions analytic in the regions  $\mathcal{D}^\pm$ , respectively,

$$\ln F^\pm(s) = \frac{1}{2\pi i} \int_{\mathcal{L}} \frac{\ln F(\zeta)}{\zeta - s} d\zeta.$$

446 Due to the analytical property of  $F(s)$  and Jordan's lemma, the integration path  
447  $\mathcal{L}$  can be closed around the upper branch cut  $\mathcal{F}^+$ . The contributions from the  
448 branch points is vanishingly small. The upper branch cut is parametrized as in  
449 Eq.(45). In the special case  $\delta = 0$ , the branch cut corresponds to the interval  
450 on the imaginary axis  $\{it, t \in [0, 1]\}$ .

451 The ratio  $\alpha(s)/\beta(s)$  appearing in the function  $F(s)$  jumps across the branch  
 452 cut according to

$$\lim_{\epsilon \rightarrow 0^+} \frac{\alpha(\zeta(t) \pm i\epsilon)}{\beta(\zeta(t) \pm i\epsilon)} = \pm i \sqrt{\frac{t}{1-t} \frac{(2-t)\delta - it}{(1-t)\delta - i(1+t)}}, \quad t \in [0, 1].$$

Eq.(45) yields

$$\ln F^-(s) = \frac{\delta + i}{2\pi i} \int_0^1 \lim_{\epsilon \rightarrow 0} [\ln F(\zeta(t) - i\epsilon) - \ln F(\zeta(t) + i\epsilon)] \frac{dt}{\zeta(t) - s},$$

and using

$$\begin{aligned} \ln F(\zeta(t) - i\epsilon) - \ln F(\zeta(t) + i\epsilon) &= \ln \frac{F(\zeta(t) - i\epsilon)}{F(\zeta(t) + i\epsilon)} \rightarrow \\ &= \ln \frac{1 - i\psi(t)}{1 + i\psi(t)} = -2i \arctan \psi(t) = -2i (\pi/2 - \arctan \psi^{-1}(t)), \end{aligned} \quad (\text{A.1})$$

453 with

$$\psi(t) = \left( \frac{(1+\eta)[(\delta+i)t - \delta]^2 - \delta^2}{(1+\eta)[(\delta+i)t - \delta]^2 + 1} \right)^2 \sqrt{\frac{(1-t)^2\delta - i(1-t^2)}{(2-t)\delta t - it^2}}, \quad (\text{A.2})$$

454 we obtain

$$\ln F^-(s) = \frac{\delta + i}{\pi} \int_0^1 \frac{\arctan \psi(t)}{\delta - (\delta + i)t + s} dt = G^-(s). \quad (\text{A.3})$$

455 In the static case  $\delta = 0$ , Eq.(A.2) gives the corresponding function introduced  
 456 in (Radi, 2008, Eq.(59))

$$\psi(t) = \frac{t^3 \sqrt{1-t^2}}{\left(t^2 - \frac{1}{\eta+1}\right)^2}.$$

457 In this situation, a pole of  $\psi(t)$  is encountered at  $t = 1/\sqrt{1+\eta}$ , inasmuch as  
 458  $\eta > 0$ , although this brings no harm to the evaluation of  $G^-(s)$ , in light of  
 459 the arctangent being bounded. In contrast, special care must be paid in the  
 460 evaluation of the contour integral when the root  $s_3$  lays inside the branch cut,  
 461 as this may bring a  $2\pi i$  jump when transforming the difference of the logarithms  
 462 in Eq.(A.1). Clearly, from Eq.(A.3) and the property (46), we have

$$F^\mp(s) = \exp G^\mp(s),$$

where  $G^\pm(-s) = G^\mp(s)$ . Observing that the factorization is independent of the location of  $s_0$  and enforcing Eq.(44) to hold at  $s = 0$  brings the requirement

$$s_0 = iabs_3 \sqrt{c \frac{F^+(0)F^-(0)}{\alpha(0)K(0)}}. \quad (\text{A.4})$$

In particular, the point  $s_0$  coincides with  $s_3$  when the function  $K(s)$  admits two pairs of roots in the physical sheet, while it is conveniently located in the branch cut when  $K(s)$  admits three root pairs.

## References

- Achenbach, J., 2012. Wave propagation in elastic solids. Vol. 16. Elsevier.
- Bleistein, N., Handelsman, R. A., 1975. Asymptotic expansions of integrals. Courier Corporation.
- Clebsch, A., 1863. Ueber die Reflexion an einer Kugelfläche. Journal für die reine und angewandte Mathematik 61, 195–262.
- Destrade, M., Fu, Y., Nobili, A., 2016. Edge wrinkling in elastically supported pre-stressed incompressible isotropic plates. Proc. R. Soc. A 472 (2193), 20160410.
- Eremeyev, V. A., Rosi, G., Naili, S., 2016. Surface/interfacial anti-plane waves in solids with surface energy. Mechanics Research Communications 74, 8–13.
- Eremeyev, V. A., Rosi, G., Naili, S., 2018. Comparison of anti-plane surface waves in strain-gradient materials and materials with surface stresses. Mathematics and Mechanics of Solids, 1081286518769960.
- Eringen, A. C., 1999. Theory of micropolar elasticity. In: Microcontinuum field theories. Springer, pp. 101–248.
- Freund, L. B., 1998. Dynamic fracture mechanics. Cambridge university press.
- Gao, X.-L., Ma, H., 2010. Solution of eshelby’s inclusion problem with a bounded domain and eshelby’s tensor for a spherical inclusion in a finite

487 spherical matrix based on a simplified strain gradient elasticity theory.  
488 Journal of the Mechanics and Physics of Solids 58 (5), 779 – 797.  
489 URL [http://www.sciencedirect.com/science/article/pii/](http://www.sciencedirect.com/science/article/pii/S0022509610000074)  
490 S0022509610000074

491 Georgiadis, H., 2003. The mode III crack problem in microstructured solids  
492 governed by dipolar gradient elasticity: static and dynamic analysis. Journal  
493 of Applied Mechanics 70 (4), 517–530.

494 Georgiadis, H., Vardoulakis, I., 1998. Anti-plane shear Lamb’s problem treated  
495 by gradient elasticity with surface energy. Wave Motion 28 (4), 353–366.

496 Georgiadis, H., Velgaki, E., 2003. High-frequency Rayleigh waves in materials  
497 with micro-structure and couple-stress effects. International Journal of Solids  
498 and Structures 40 (10), 2501–2520.

499 Gourgiotis, P., Georgiadis, H., Neocleous, I., 2013. On the reflection of waves in  
500 half-spaces of microstructured materials governed by dipolar gradient elastic-  
501 ity. Wave Motion 50 (3), 437–455.

502 Graff, K., Pao, Y.-H., 1967. The effects of couple-stresses on the propagation  
503 and reflection of plane waves in an elastic half-space. Journal of Sound and  
504 Vibration 6 (2), 217–229.

505 Kaplunov, J., Nobili, A., 2017. A robust approach for analysing dispersion of  
506 elastic waves in an orthotropic cylindrical shell. Journal of Sound and Vibra-  
507 tion 401, 23–35.

508 Koiter, W., 1964. Couple-stress in the theory of elasticity. In: Proc. K. Ned.  
509 Akad. Wet. Vol. 67. North Holland Pub, pp. 17–44.

510 Lakes, R., 1986. Experimental microelasticity of two porous solids. International  
511 Journal of Solids and Structures 22 (1), 55–63.

512 Lam, D. C., Yang, F., Chong, A., Wang, J., Tong, P., 2003. Experiments and  
513 theory in strain gradient elasticity. Journal of the Mechanics and Physics of  
514 Solids 51 (8), 1477–1508.

515 Maranganti, R., Sharma, P., 2007. A novel atomistic approach to determine  
516 strain-gradient elasticity constants: Tabulation and comparison for various  
517 metals, semiconductors, silica, polymers and the (ir) relevance for nanotech-  
518 nologies. *Journal of the Mechanics and Physics of Solids* 55 (9), 1823–1852.

519 Mindlin, R., Eshel, N., 1968. On first strain-gradient theories in linear elasticity.  
520 *International Journal of Solids and Structures* 4 (1), 109–124.

521 Mindlin, R. D., 1964. Micro-structure in linear elasticity. *Archive for Rational*  
522 *Mechanics and Analysis* 16 (1), 51–78.

523 Mishuris, G., Piccolroaz, A., Radi, E., 2012. Steady-state propagation of a mode  
524 III crack in couple stress elastic materials. *International Journal of Engineer-*  
525 *ing Science* 61, 112–128.

526 Morini, L., Piccolroaz, A., Mishuris, G., 2014. Remarks on the energy release  
527 rate for an antiplane moving crack in couple stress elasticity. *International*  
528 *Journal of Solids and Structures* 51 (18), 3087–3100.

529 Morini, L., Piccolroaz, A., Mishuris, G., Radi, E., 2013. On fracture criteria for  
530 dynamic crack propagation in elastic materials with couple stresses. *Interna-*  
531 *tional Journal of Engineering Science* 71, 45–61.

532 Mow, C.-C., Pao, Y.-H., 1971. The diffraction of elastic waves and dynamic  
533 stress concentrations. Tech. rep., RAND CORP SANTA MONICA CALIF.

534 Nakamura, S., Lakes, R., 1995. Finite element analysis of Saint-Venant end  
535 effects in micropolar elastic solids. *Engineering Computations* 12 (6), 571–  
536 587.

537 Nobili, A., Radi, E., Lanzoni, L., 2017. Flexural edge waves generated by steady-  
538 state propagation of a loaded rectilinear crack in an elastically supported thin  
539 plate. In: *Proc. R. Soc. A. Vol. 473. The Royal Society*, p. 20170265.

540 Noble, B., 1958. Methods based on the Wiener-Hopf technique for the solution  
541 of partial differential equations, *International Series of Monographs on Pure*  
542 *and Applied Mathematics. Vol. 7. Pergamon Press, New York.*

- 543 Ottosen, N. S., Ristinmaa, M., Ljung, C., 2000. Rayleigh waves obtained by the  
544 indeterminate couple-stress theory. *European Journal of Mechanics-A/Solids*  
545 19 (6), 929–947.
- 546 Radi, E., 2008. On the effects of characteristic lengths in bending and torsion  
547 on mode iii crack in couple stress elasticity. *International Journal of Solids*  
548 *and Structures* 45 (10), 3033–3058.
- 549 Rayleigh, J., 1896. *The theory of sound*. Macmillan.
- 550 Roos, B. W., 1969. *Analytic functions and distributions in physics and engi-*  
551 *neering*.
- 552 Shodja, H., Goodarzi, A., Delfani, M., Haftbaradaran, H., 2015. Scattering of an  
553 anti-plane shear wave by an embedded cylindrical micro-/nano-fiber within  
554 couple stress theory with micro inertia. *International Journal of Solids and*  
555 *Structures* 58, 73–90.
- 556 Yang, F., Chong, A., Lam, D. C. C., Tong, P., 2002. Couple stress based strain  
557 gradient theory for elasticity. *International Journal of Solids and Structures*  
558 39 (10), 2731–2743.
- 559 Zhang, L., Huang, Y., Chen, J., Hwang, K., 1998. The mode III full-field solu-  
560 tion in elastic materials with strain gradient effects. *International Journal of*  
561 *Fracture* 92 (4), 325–348.